Sequentially firing neurons confer flexible timing in neural pattern generators

Alexander Urban
Department of Physics, University of Pittsburgh, 100 Allen Hall, 3941 O'Hara Street, Pittsburgh, Pennsylvania 15260, USA

Bard Ermentrout
Department of Mathematics, University of Pittsburgh, 139 University Place, Pittsburgh, Pennsylvania 15260, USA

(Received 26 August 2010; revised manuscript received 19 January 2011; published 16 May 2011)

Neuronal networks exhibit a variety of complex spatiotemporal patterns that include sequential activity, synchrony, and wavelike dynamics. Inhibition is the primary means through which such patterns are implemented. This behavior is dependent on both the intrinsic dynamics of the individual neurons as well as the connectivity patterns. Many neural circuits consist of networks of smaller subcircuits (motifs) that are coupled together to form the larger system. In this paper, we consider a particularly simple motif, comprising purely inhibitory interactions, which generates sequential periodic dynamics. We first describe the dynamics of the single motif both for general balanced coupling (all cells receive the same number and strength of inputs) and then for a specific class of balanced networks: circulant systems. We couple these motifs together to form larger networks. We use the theory of weak coupling to derive phase models which, themselves, have a certain structure and symmetry. We show that this structure endows the coupled system with the ability to produce arbitrary timing relationships between symmetrically coupled motifs and that the phase relationships are robust over a wide range of frequencies. The theory is applicable to many other systems in biology and physics.

DOI: 10.1103/PhysRevE.83.051914 PACS number(s): 87.18.Sn, 84.35.+i

I. INTRODUCTION

Biological systems and, in particular, many nervous systems are organized around repetitions of simple motifs [1,2]. One of the goals of theoretical biology and computational neuroscience is to understand the behavior and dynamics of the whole system given the dynamics of the parts and their connectivity. Specifically, a common question is how the connections between the parts determine the output of the coupled network. For example, many invertebrate nervous systems are composed of small (often as few as three cells) motifs which generate rhythmic dynamics [3–6]. These motifs are then coupled together (for example, as left and right pairs or in a chain) to form larger networks. The full network is responsible for producing the correct neural inputs to various motor functions responsible for swimming [7–9], walking [10,11], and eating [4]. These oscillatory motifs are not restricted to invertebrates, but have also been found in vertebrates [12].

Our choice of motifs is motivated by a number of other neural models where the connections between units are dominated by inhibition. Winner-less-competition (WLC) networks [13] represent a class of such networks which have been shown to generate complex patterned sequences. They have been successfully used to model the dynamics observed in the insect olfactory system as well as in some central pattern generators (CPGs) [14]. While many inhibitory networks produce WLC via heteroclinic cycles, this is not always the only type of behavior found. Standard WLC examples such as the Lotka-Volterra system are also able to generate limit cycle oscillations. Indeed, Terman *et al*. [15] consider a class of motifs that are also dominated asymmetric inhibition. There, they consider networks of relaxation oscillators in which the activity of one suppresses the activity of all other cells to which it is connected. Once the active cell turns off, some other cell or cells turn on and so on. Their motifs settle into attracting periodic orbits.

Winner-take-all (WTA) networks are characterized by symmetric coupling and thus they tend to generate fixed-point behavior. In contrast, random networks and the kinds of networks encountered in neural contexts [2,16,17] are far from symmetric, so that such networks can often produce temporally rich behavior such as limit cycles and chaos [13]. Furthermore, unlike fixed-point-generating networks, small coupling strengths can have dramatic effects in periodic and chaotic networks. Specifically, when an isolated motif produces stable fixed-point behavior, then coupling between two such motifs must be sufficiently strong to produce qualitative changes from the uncoupled system. In contrast, chaotic and oscillatory motifs can be strongly influenced by weak interactions.

The goal of this paper is to first analyze a particular class of motifs and show that rhythmic sequential dynamics arise generically in a wide variety of circumstances. Second, we then ask what type of dynamics arises when such oscillatory motifs are coupled together in a symmetric manner. Since the relative timing of neuronal circuit output (oscillatory and otherwise) is quite important (particularly for rhythmic motor systems, but also for sensory systems [18]), we ask how the coupling between a pair of oscillatory motifs affects the relative timing of their outputs. We use bifurcation theory to study the onset of oscillatory dynamics in the individual motif. We then use the theory of averaging and weak coupling to study the relative timing of outputs between pairs of such modular networks. We compare the weak-coupling phase models with the full model. We finally show that the use of sequence-generating modules confers the coupled network with robust timing relationships over a wide range of frequencies, a property that is especially important in CPGs.

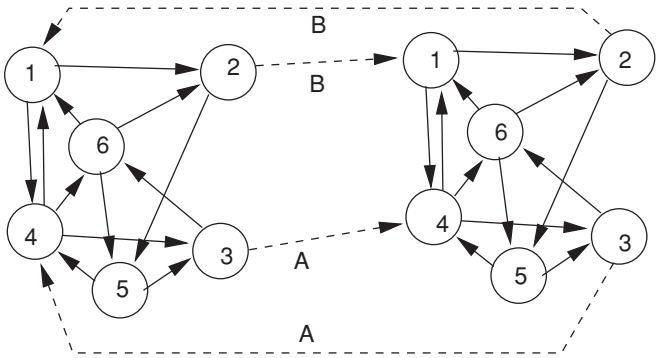

FIG. 1. Two mutually coupled networks. Solid lines are intranetwork connections and can be general. Dashed lines show two types of connections A,B which are reciprocal. Note that within the network, the coupling is "balanced": Each cell receives the same number of inputs.

II. PURE INHIBITORY NEURAL MODELS

Figure 1 shows a pair of coupled motifs, each of which is a network of five coupled cells. Suppose that the isolated motif produces oscillatory but not necessarily synchronous behavior. That is, say that the cells within the motif have different (perhaps just time-shifted) wave forms. Then we can ask, what happens when the two motifs are coupled and how does the resulting dynamics depend on the choice of connections, A or B or some combination of both of them. For example, the two motifs could represent the left and right sides of a bilateral CPG with the dashed lines representing the cross coupling. In order to address this question, we analyze the dynamics within a single motif in which all connections are inhibitory. We look for architectures that generate stable sequential rhythmic dynamics. We start with general random networks and show that periodic dynamics are quite common and can be understood from the spectra of the connectivity matrices. We find that a common pattern of activity consists of three or more cells alternating their dynamics. This suggests a simpler class of models, circulant systems, which show robust periodic dynamics as the drive or the coupling strength increase. Finally, we turn to the simplest circulant system of three cells that inhibit each other asymmetrically. This particular motif is remarkably common in neuroscience and is the basis for many of the CPGs discussed in the Introduction.

A. Random balanced coupling

There are many ways to choose the dynamics within a motif and, indeed, even the dynamics within each of the cells composing the motif. We will use a simple firing rate Wilson-Cowan model for each cell within a motif and we will couple cells with inhibitory coupling. Thus each motif has the form

$$\dot{x}_i = -x_i + F\left(I_i - \sum_{k=1}^{n} g_{ik}x_k\right), \tag{1}$$

where I_i is the input into the ith cell, g_{ik} is the strength of interaction between cell k and cell i, and $F(u)$ is a monotonically increasing function; we will use $F(u) = 1/[1 + \exp(-u)]$. The coupling strengths g_{ik} are non-negative.

The dynamics of even as simple a network as (1) can be complicated. To get a handle on it, we will consider motifs that are homogeneous; that is, all the applied inputs I_i are identical and the net input into each cell is the same:

$$\sum_{k=1}^{n} g_{ik} = g, \quad \text{for all } i.$$

With this assumption, it is immediately clear that there is a unique homogeneous fixed point, $x_i = \bar{u}$, where

$$\bar{u} = F(I - g\bar{u}).$$

The network illustrated in Fig. 1 has the so-called *balanced* property; that is, the total inputs coming into any cell is the same for each cell. There are several ways to achieve balance in a network. For example, each cell could receive the same number of inputs where each have the same strength. More generally, the summed strength of all inputs to each cell could be the same with no constraints on who is coupled to whom. Balanced systems have been the subject of a great deal of recent work [19,20].

We write $g_{ik} = gG_{ik}$, where G_{ik} is now fixed and is such that $\sum_{k=1}^{n} G_{ik} = 1$. Thus, g and the input I are the two parameters in our network. We can now ask what happens as these parameters change. Thus, we perform a local stability analysis around the homogeneous equilibrium point, $x_i = \bar{u}$. Let $\alpha := F'(I - g\bar{u})$, where $F'(u)$ is derivative of F. $\bar{u}$ is itself a function of g and I, decreasing as a function of g and increasing as a function of I. Thus, α is also a function of g,I so that as g or I change, so does the parameter α. Since F is monotonic, α is always positive and is maximal at the inflection point of F. For our choice of F, the inflection point is at 0. Finally, we can always choose I so that $\bar{u}$ is at the inflection point, for our function, $I = g/2$ guarantees this feature.

With these preliminary remarks, we can write down the linearized equation

$$\dot{y}_i = -y_i - \alpha g \sum_{k=1}^{n} G_{ik}y_k.$$

Let μ_j be an eigenvalue of the matrix G whose entries are G_{ik}. Then, the eigenvalues of the linearized system above are

$$\lambda_j = -1 + \alpha g \mu_j.$$

As noted above, we can always move along a parameter path in g,I so that α is some fixed positive value. Thus, we can make the quantity αg as large as we would like by increasing g and choosing I appropriately. The eigenvalues λ_j are clearly negative for g sufficiently small. G is the transpose of a probability matrix: All entries are non-negative and the row sums are 1. We can conclude that the eigenvalue of G that has maximum magnitude is 1 with an eigenvector of all 1's. This gives, for the linearized system, an eigenvalue $\lambda = -1 - g\alpha$, which is clearly negative. Let ν be the eigenvalue of G which has the most negative real part. Let us write $\nu = -r \pm i\omega$. Then as g increases, the linearized system has an eigenvalue

$$\lambda = -1 + \alpha g r - i\alpha g\omega.$$

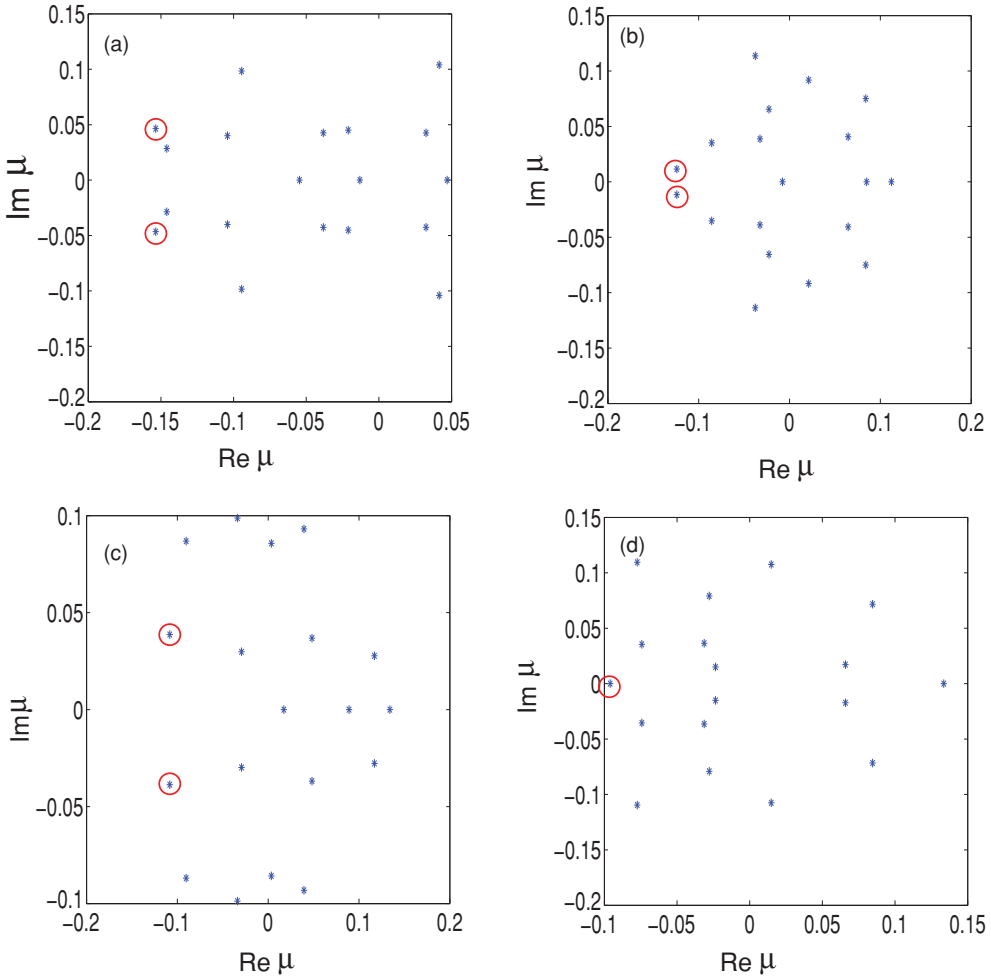

FIG. 2. (Color online) Eigenvalue spectra of several 20×20 random matrices with row sums equal to 1. In addition to the 19 eigenvalues shown, there is a simple eigenvalue, $\lambda = 1$, that is not shown. The entries of each matrix are chosen to be uniformly distributed on $(0,1)$ and then each row is scaled so the row sum is 1. (a)–(d) are four such randomly chosen matrices.

If $g > 1/(\alpha r)$, then the real part of λ becomes positive. If this particular eigenvalue is complex ($\omega \neq 0$), then we generically expect a Hopf bifurcation to occur. Of course, if the matrix G is symmetric, then the only long-time solutions to (1) are fixed points. Thus, to get sequencelike behavior for such purely inhibitory networks requires that the matrix G be nonsymmetric. Figure 2 shows examples of several 20×20 random matrices. We see that in Figs. 2(a), 2(b), and 2(c) the eigenvalue with the most negative real part is complex (circles) while in Fig. 2(d) the most negative eigenvalue is real. From our prior discussion, as g increases, we expect to see the loss of stability of the constant steady state via a Hopf bifurcation in the examples shown in Figs. 2(a), 2(b), and 2(c), but a pitchfork bifurcation with the matrix example in Fig. 2(d). In general, for an $m \times m$ random matrix with entries taken from a uniform distribution and row sums normalized to 1, the $m-1$ eigenvalues that are not 1 lie in a circle of radius $1/\sqrt{m}$ [21]. Thus, we need to choose only those matrices whose eigenvalues with the most negative real parts are also complex.

We have sketched out the linear theory for these inhibitory networks, but we are interested in the oscillatory dynamics, so we will resort to a numerical computation of the bifurcation diagrams as the coupling strength g increases. Figure 3 shows the bifurcation diagram for the system with the matrix in Fig. 2(a) and $I = 20$. As predicted from the spectrum of G, the uniform steady state loses stability through a Hopf bifurcation at a value of g near 30. There is a supercritical branch of periodic solutions that bifurcates (shown by the thick lines) which appears to terminate at a saddle homoclinic orbit. Figure 3(c) shows that the frequency rapidly drops to 0 as g increases toward the homoclinic. The nearly vertical frequency drop suggests a saddle homoclinic rather than a saddle node on an invariant circle (SNIC) which, instead, shows a square-root dependence of the frequency. Figure 3(b) shows a two-parameter diagram, that is, the curve of Hopf bifurcations as I and g co-vary. For quite a wide range of applied currents, we see that there is a Hopf bifurcation to periodic orbits as the linear analysis suggests. Figure 3(d) shows the projection of the trajectories of three different cells in the 20-cell network. One point that we would like to emphasize and is clear from Fig. 3(d) is the sequential nature of the firing. That is, during a cycle, each of the three variables shown comes on at different phases.

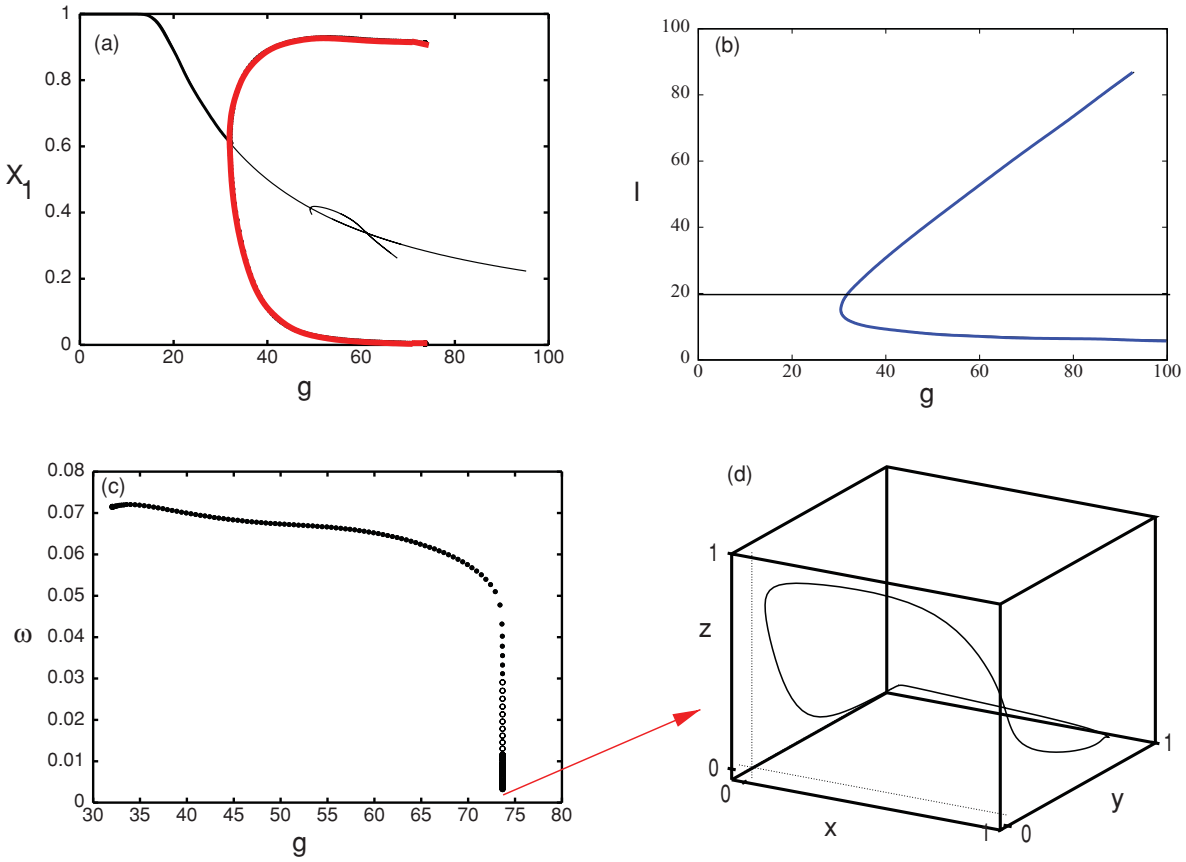

FIG. 3. (Color online) (a) Bifurcation diagram for a 20-neuron network as g varies with $I = 20$. The solid thick black line represents the symmetric stable equilibrium and the light curve is the branch of periodic orbits. An unstable pitchfork bifurcation to unstable equilibria is partially shown between $g = 50$ and $g = 70$. (b) Two-parameter diagram with I and g as parameters. The black line represents the parameters for (a). The lighter colored curve is the curve of Hopf bifurcations. (c) Frequency of oscillation from (a). (d) Projection of x_9,x_{16},x_{18} near termination of the branch of periodic orbits in (c).

Figure 4 shows additional bifurcation diagrams for twenty cell random networks. Figure 4(a) depicts the dynamics beyond the bifurcation for the coupling whose eigenvalue spectrum is shown in Fig. 2(b). As Fig. 3, the oscillation persists for a wide range of applied currents I with apparently no additional bifurcations. This is in contrast to the behavior of the system whose eigenspectrum is shown in Fig. 2(c) and whose bifurcation diagrams are depicted in Figs. 4(b)–4(d) for three different applied currents. First, we note that, as predicted from the linear theory, all three systems undergo Hopf bifurcations as the coupling strength g is increased. However, the dynamics past the Hopf bifurcation depends very strongly on the applied current I. When $I = 20$, then, as Fig. 4(a), the oscillation persists for very large values of g, but the limit cycle undergoes some complex bifurcations for $g \approx 55$ before returning to a simple limit cycle. Choosing $I = 30,10$ leads to dramatic differences in the global dynamics. For both $I = 10,30$ but not $I = 20$, the oscillation terminates at a SNIC formed by a stable and unstable pair of fixed points (light colored arrows). However, at low drive, ($I = 10$), there is a small regime of synaptic strengths where there are two small-amplitude stable periodic orbits (green arrow).

Figure 5 shows that it is not even necessary that the initial bifurcation be a Hopf in order to get oscillatory dynamics. Figure 2(d) shows a connection matrix where the eigenvalue with most negative real part is real, so that a pitchfork bifurcation is predicted from the matrix. As can be seen in the bifurcation diagram, the uniform fixed point loses stability at a pitchfork bifurcation (a). The lower branch of fixed points undergoes a Hopf bifurcation (b), which terminates on a SNIC (c). The upper branch undergoes a Hopf bifurcation at two points (d), (e). Another pitchfork emerges (f) which is unstable, but the lower branch stabilizes at a saddle node (g) and produces a Hopf bifurcation (h). Thus for g between points (c) and (h), there are three stable limit cycles. The black arrow shows the point which we will explore later in the next section as the oscillation is simple yet quite rich in structure. (By rich, we mean that it is not too close to a pure sinusoidal oscillation and has several large Fourier components.)

B. Circulant matrices

Perhaps the easiest way to connect a network of cells in order to produce an oscillation or other patterned state is to assume that the coupling matrix G_{ij} is a function of $i - j$ only. We also assume that the coupling is not isotropic, for then $G = G^T$ and all eigenvalues of G will be real. The resulting

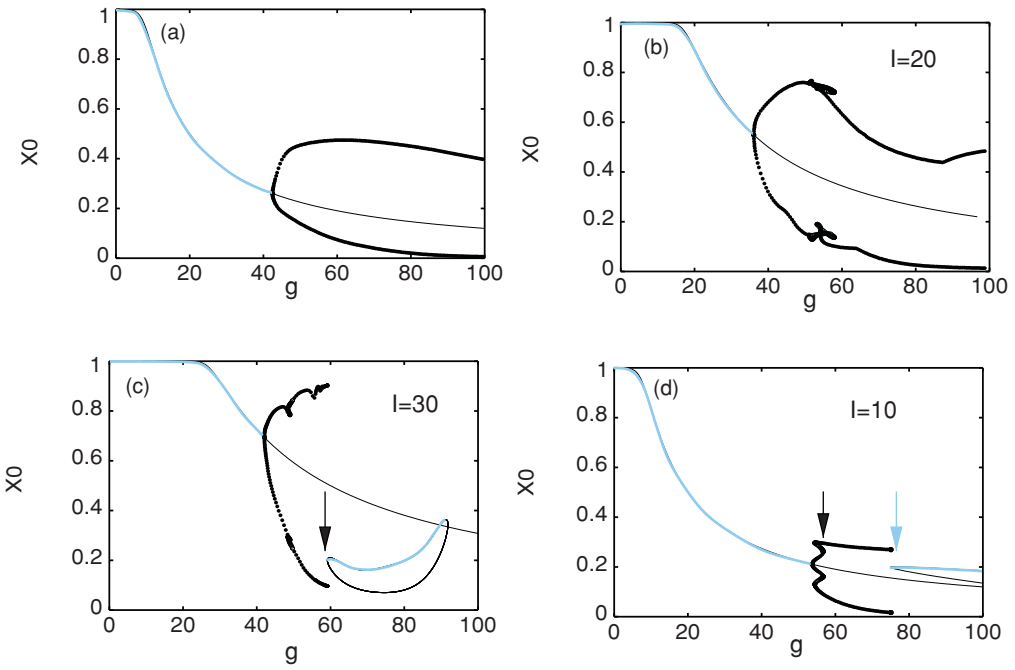

FIG. 4. (Color online) Different 20-neuron networks. (a) Similar to Fig. 3 with the weight matrix from Fig. 2(b). (b)–(d) Weight matrix from Fig. 2(c), with three different values of I. Light curves are stable fixed points, thin black are unstable, and thick dark curves are limit cycles. Light colored arrows mark SNIC bifurcations and the black arrow marks a pair of small-amplitude stable limit cycles.

network is then a gradient system [22] and all solutions tend to equilibria. Thus, while we assume G_{ij} is a function of $i-j$, it is not a function of $|i-j|$. Finally, we assume the connectivity is topologically equivalent to a circle. This kind of system arises naturally in networks that have some type of spatial organization, such as the "ring model" [23]. Matrices of this form are called circulant. We write the first row of G as

$$R_1 := [a_0, a_1, \ldots, a_{N-1}]$$

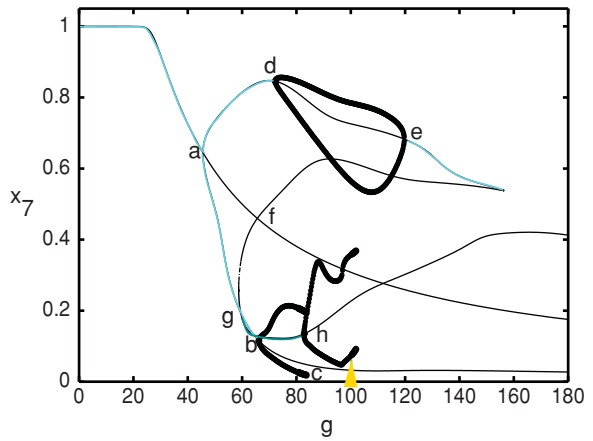

FIG. 5. (Color online) Bifurcation diagram of the system corresponding to Fig. 2(d), where the first instability is at a zero eigenvalue resulting in a pitchfork (a) in the figure. Light curves are stable equilibria, thin black curves are unstable equilibria, and thick curves are stable periodic orbits. Here $I = 30$. Arrow denotes parameters used in Fig. 14.

and suppose that the second row is the same as the first row, shifted to the right:

$$R_2 := [a_{N-1}, a_0, a_1, a_2, \ldots, a_{N-2}].$$

We similarly shift the other rows to obtain the full matrix. For such matrices, the eigenvalues are explicitly computable:

$$\mu_k = \sum_{j=0}^{m-1} a_j e^{-2\pi i j k/m}. \tag{2}$$

Thus, if $a_j \neq a_{m-j}$, then we expect the eigenvalues will be complex (except $k = 0$, the dominant positive eigenvalue). The number k is called the wave number for the eigenvalue. Figure 6 shows an example of the dynamics of a 20-neuron system with R_1 randomly chosen. Figure 6(a) shows the eigenvalue spectrum. The bifurcation diagram in Fig. 6(b) shows a single stable branch of periodic orbits emerging from the uniform state. The pattern of oscillations is shown in Fig. 6(c). The spatial mode is $2\pi 3/20$, that is, $k = 3$. Since 3 and 20 are relatively prime, no two oscillators are at their maximum at the same time. The resulting pattern is a wave that has three oscillators near their maximum at any given time.

What is crucial for our ensuing analysis is that the network of cells generates oscillations in which different members come on during different parts of the cycle. In the example in Fig. 6(c), seven groups of three oscillators occur in succession. The simplest network capable of producing sequential activity is a three-cell circulant system:

$$\begin{aligned} x_1' &= -x_1 + F(I - g[ax_1 + bx_2 + cx_3]), \\ x_2' &= -x_2 + F(I - g[ax_2 + bx_3 + cx_1]), \\ x_3' &= -x_3 + F(I - g[ax_3 + bx_1 + cx_2]). \end{aligned} \tag{3}$$

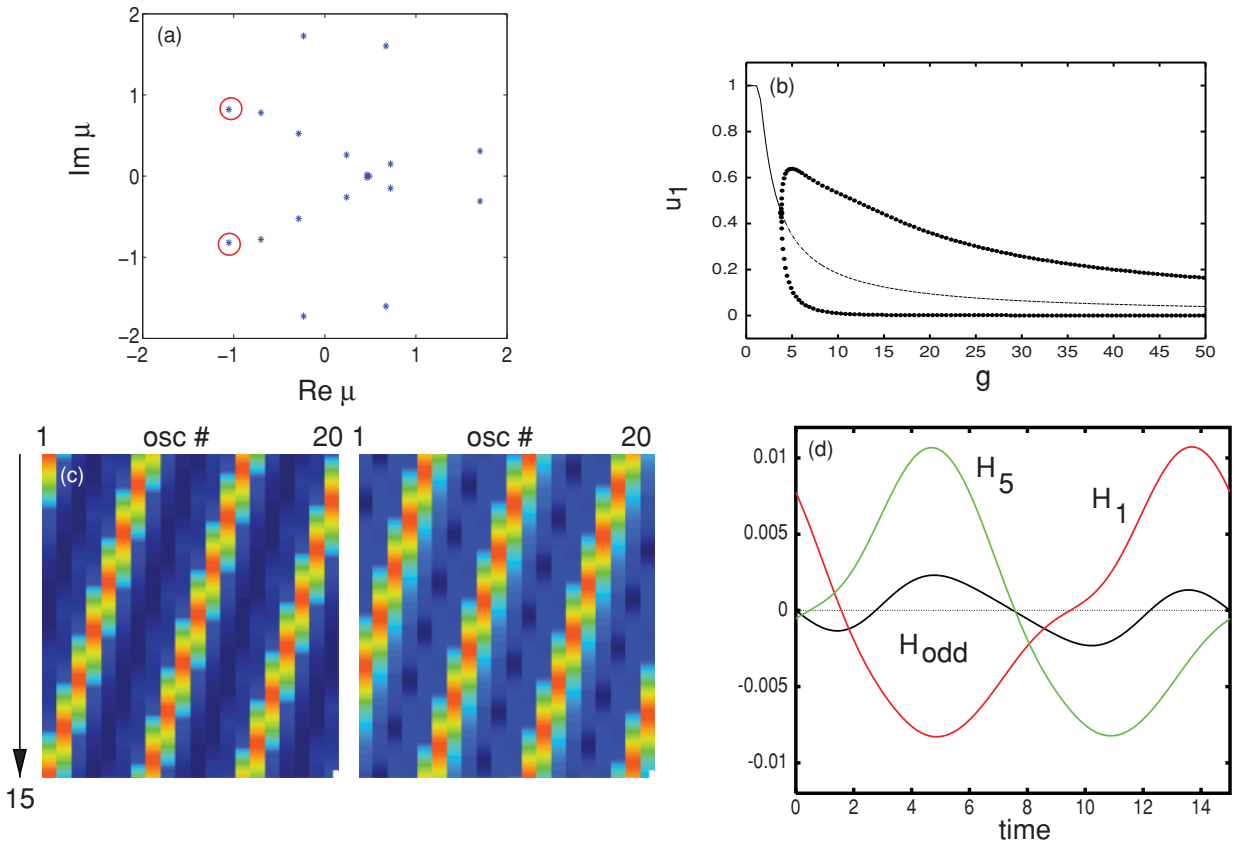

FIG. 6. (Color online) 20-neuron circulant system. (a) Eigenvalue spectrum. (b) Bifurcation diagram showing a single primary branch of periodic orbits ($I = 20$). (c) Left-hand side: "Space-time" plot of dynamics for $g = 18$. Dominant spatial mode is $2\pi(3/20)$. Right-hand side: Phase sensitivity for one cycle of the oscillation. (d) Interaction functions when oscillator 1 receives inputs from oscillators 1 or 5 from the other motif. The black curve is the odd part of the interaction function when inputs from 1 and 5 are equal in strength. [See Eq. (4) for the definition of H.]

Here a,b,c are non-negative parameters. Typically, we take $0 < a < b < c$. Figure 7 shows a figure analogous to Fig. 3 for this network. Unlike the 20-neuron case, we can gain a fairly complete understanding of the behavior. The periodic orbit emerges super-critically from the symmetric equilibrium point and terminates on a saddle-node bifurcation of equilibria. These equilibria correspond to states in which each of the three neurons is the "winner." The two-parameter diagram [Fig. 7(b)] is almost the same as the 20-neuron network, but the termination is on a symmetric SNIC rather than a saddle homoclinic. The frequency shows the characteristic square-root shape of a saddle node on a limit cycle bifurcation [Fig. 7(c)] and the projected orbit clearly shows the "ghosts" of the three asymmetric fixed points that disappear at the triple saddle-node bifurcation. Three-cell networks are very common in vertebrate CPGs, as discussed in the Introduction to this paper. Rabinovich has analyzed a similar system to this. However, his system produces a heteroclinic cycle.

In this section, we have shown that driven inhibitory networks of the form (1) generically produce limit cycle oscillations in which the cells in the network alternate their activity. In other words, as the three-neuron model analyzed in Ref. [14], these more general networks produce repetitive sequential activity. Using such a network as our basic motif, we now explore the dynamical possibilities of coupling them together. Given that the cells are "on" at different parts of their cycle, we expect that there can be many different patterns of synchrony and locking depending on which cell is connected to which.

III. WEAK-COUPLING THEORY

The dynamics of generally coupled oscillators is a difficult problem, so that several approaches can be taken to make the problem tractable. One of the most general methods available is to restrict the analysis to the case where interactions between the oscillators are "weak." That is, coupling is not so strong as to distort the individual limit cycles. We first summarize the Malkin theorem for weak coupling [24].

Consider

$$X' = Q(X) + \epsilon C_1(X,Y) + O(\epsilon^2),$$
$$Y' = Q(Y) + \epsilon C_2(Y,X) + O(\epsilon^2).$$

Here $Q : R^n \to R^n$ and $C_k : R^n \times R^n \to R^n$ are smooth functions. We assume that there is an asymptotically stable limit cycle, $X_0(t)$ for the uncoupled system, $X_0' = Q(X_0)$

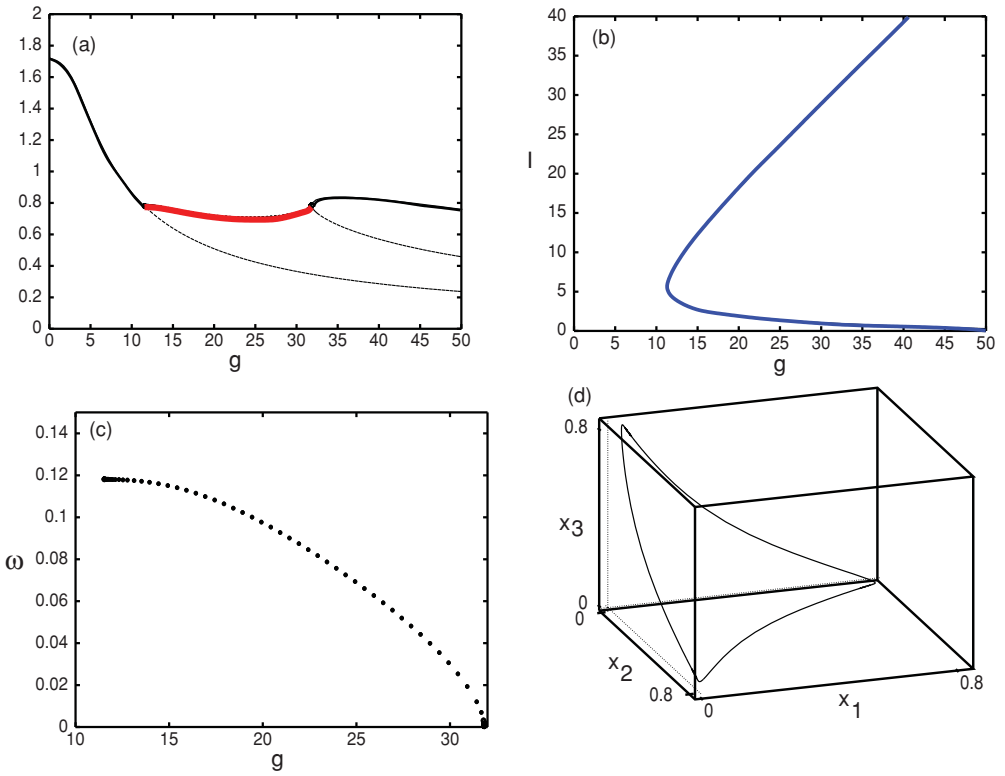

FIG. 7. (Color online) Three-neuron network, $a = 0.1$, $b = 0.3$, $c = 0.6$, $I = 5$ with circulant structure. (a) Bifurcation diagram showing the L^2 norm. (b) Two-parameter diagram showing the curve of Hopf bifurcations. (c) Frequency of oscillations. (d) Three-dimensional projection for $g = 31$ near the termination of the branch of periodics.

with period P. $C_{1,2}$ represent the coupling functions to order $0 < \epsilon \ll 1$. Let $X^*(t)$ satisfy

$$\frac{dX^*}{dt} = -D_X Q[X_0(t)]^T X^*, \quad X^*(t)X_0'(t) = 1.$$

Here $D_X Q[X_0(t)]$ is the $N \times N$ Jacobi matrix [of partial derivatives of Q evaluated along the limit cycle, $X_0(t)$]. Then $X(t) = X_0(\theta_X) + O(\epsilon)$, $Y(t) = X_0(\theta_Y) + O(\epsilon)$, and

$$\frac{d\theta_X}{dt} = 1 + \epsilon H_1(\theta_Y - \theta_X) + O(\epsilon^2),$$
$$\frac{d\theta_Y}{dt} = 1 + \epsilon H_2(\theta_X - \theta_Y) + O(\epsilon^2),$$

where

$$H_j(\phi) := \frac{1}{P}\int_0^P X^*(t)C_j[X_0(t), X_0(t+\phi)]dt. \qquad (4)$$

The function $X^*(t)$ is called the sensitivity function or the adjoint solution.

Before turning to the application of this theory to our motifs, we show why understanding the interaction functions $H_j(\phi)$ is useful. For reciprocally coupled identical oscillators, the Malkin theorem implies (to order ϵ)

$$\frac{d\theta_X}{dt} = 1 + \epsilon H(\theta_Y - \theta_X),$$
$$\frac{d\theta_Y}{dt} = 1 + \epsilon H(\theta_X - \theta_Y).$$

Let $\phi := \theta_Y - \theta_X$. Then

$$\frac{d\phi}{dt} = -2\epsilon H_{\text{odd}}(\phi) := \epsilon[H(-\phi) - H(\phi)].$$

Any continuous odd periodic function has at least two zeros, $\phi = 0$ and $\phi = P/2$. The former is the perfectly synchronous solution where both of the motifs follow the same exact trajectory and the latter is the "antiphase" solution where the motifs are half a cycle apart. The existence of these solutions is independent of the nature of the coupling between two motifs, however, their stability does depend on the coupling, as we will show shortly. There is no reason why $H_{\text{odd}}(\phi)$, might not have other zeros besides $0, P/2$. Such a zero would be very sensitive to the precise nature of the coupling and, if the zero is stable, would confer a great deal of flexibility in the range of stable patterns between two or more coupled motifs. Near the Hopf bifurcation, the limit cycles are very sinusoidal and thus they have only a single Fourier component. Their sensitivity has a similar sinusoidal form so that their odd part of the interaction function is proportional to $\sin 2\pi\phi/P$ [25]. This means that the only possible patterns are $\phi = 0, P/2$. For this reason, we want to move away from the Hopf bifurcation point so that the limit cycle $X_0(t)$ and the sensitivity function $X^*(t)$ have multiple Fourier modes. We conclude by remarking that perfect synchrony, $\phi = 0$, is stable if $-2H'_{\text{odd}}(0) = -2H'(0)$ is negative. That is, when $H'(0) > 0$. Similarly, the antiphase solution, $\phi = P/2$, is stable when $H'(P/2) > 0$.

A. Weakly coupled motifs

We now apply the weak-coupling theory to a pair of coupled motifs where the coupling strength, ϵ is small:

$$x_i' = -x_i + f\left(I - g\sum_{j=1}^{m} G_{ij}x_j - \epsilon\sum_{j=1}^{m} C_{ij}y_j\right),$$

$$y_i' = -y_i + f\left(I - g\sum_{j=1}^{m} G_{ij}y_j - \epsilon\sum_{j=1}^{m} C_{ij}x_j\right).$$

We expand the inside of f in terms of ϵ to find

$$\begin{aligned} x_i' &= -x_i + f\left(I - g\sum_{j=1}^{m} G_{ij}x_j - \epsilon\sum_{j=1}^{m} C_{ij}y_j\right) \\ &= -x_i + f(S_i) - \epsilon f'(S_i)\sum_{j=1}^{m} C_{ij}y_j + O(\epsilon^2), \end{aligned} \quad (5)$$

where $S_i = I - g\sum_{j=1}^{m} G_{ij}x_j$. The equations for y_i are similarly defined with the y and x interchanged. For the remainder of the paper, we suppose the coupling between motifs is symmetric as in Fig. 1. Let $x_i^*(t)$ denote the components of $X^*(t)$ and $x_i(t)$ denote the components of $X_0(t)$. Then

$$H(\phi) = -\frac{1}{P}\int_0^P \left[\sum_{i,j=1}^{m} x_i^*(t)f'[S_i(t)]C_{ij}x_j(t+\phi)\right]dt. \quad (6)$$

Let us define $z_i(t) = x_i^*(t)f'[S_i(t)]$. This function determines the sensitivity of the oscillator to perturbations of the ith cell. Then, we can write (6) as

$$H(\phi) = -\frac{1}{P}\int_0^P \left[\sum_{i,j=1}^{m} z_i(t)C_{ij}x_j(t+\phi)\right]dt.$$

Thus, the interaction function H is dependent on the sensitivity of the receiver and the activity of the sender. For example, if some of cells do not participate in the rhythm, that is, they are either suppressed or nearly in the maximally active state, then they will be insensitive as receivers (since $f'[S_i(t)]$ is close to zero) nor will they be useful senders since $x_i(t)$ is nearly constant and thus conveys no phase information. Generally speaking, in dealing with inhibitory motifs that have no special structure, some fraction of the cells will not participate in the rhythm in the sense that their activities only fluctuate weakly. In circulant systems, all cells participate in the rhythm and their wave forms are just shifted versions of each other, so all of them are equally good at sending and receiving inputs from other motifs.

B. General results about synchrony

Before our analysis of specific motifs and patterns of coupling, we look at synchrony with a particular kind of coupling. Consider

$$x_i' = -x_i + F\left(I - g\sum_{j} G_{ij}x_j - \epsilon\sum_{j} C_{ij}y_j\right). \quad (7)$$

The general interaction function is given by

$$H(\phi) = -\frac{1}{T}\int_0^T X^*(t)\cdot F'(I - gGX(t))CX(t+\phi)dt. \quad (8)$$

Here $F'(\cdot)$ means the vector formed from each of the components, $F'(I - \sum_j G_{ij}X_i(t))$. Synchrony is stable if $H'(0) > 0$, that is,

$$M := -\frac{1}{T}\int_0^T X^*(t)\cdot F'(I - gGX(t))CX'(t), \quad dt > 0. \quad (9)$$

Consider the equation

$$X' + X = F(I - gGX). \quad (10)$$

Differentiate this with respect to t and we obtain

$$X'' + X' = -gF'(I - gGX)GX'.$$

Integrate this against the adjoint $X^*(t)$ using the fact that $X'(t)\cdot X^*(t) = 1$ to obtain

$$\begin{aligned} 1 + \frac{1}{P}\int_0^P X^*(t)\cdot X''(t)dt \\ = -g\frac{1}{P}\int_0^P X^*(t)\cdot F'(I - gGX(t))GX'(t)dt. \end{aligned} \quad (11)$$

If the coupling to other groups, C is exactly the same as the coupling within groups, G, then we see that

$$gH'(0) = 1 + \frac{1}{T}\int_0^T X^*(t)\cdot X''(t)dt. \quad (12)$$

The term involving $X''(t)$ arises in many situations, for example, in the evolution of the phase for reaction-diffusion equations with scalar coupling [26]. It will be small or zero if the isochrons of the limit cycle are nearly radial (small "twist," see below). Thus, while it is not possible to declare that $H'(0)$ is positive, for a generic class of limit cycles, the twist is small. At a SNIC, the integral vanishes (see below). Thus, for our three-oscillator circulant system (which is near the SNIC), we expect that synchrony will be stable if the coupling between groups exactly reflects the coupling within the group and is simply weaker.

We now prove that near a SNIC, the integral vanishes. The normal form near a SNIC is [27]

$$x' = 1 - \cos x + a^2(1 + \cos x).$$

We can solve this for the periodic orbit, $x(t) = -2\arctan[a\cot(at)]$. As this is a scalar equation, the adjoint is $x^*(t) = 1/x'(t)$. Since $x'(t)$ is an even periodic function, the adjoint is also an even periodic function and $x''(t)$ is an odd periodic function. Thus, the integral of $x''(t)x^*(t)$ vanishes. Hence, near a SNIC, we have that $H'(0) > 0$ and synchrony is stable.

Near a Hopf bifurcation, $X(t) = (\cos t, \sin t)$ and $X^*(t) = (q\cos t - \sin t, \cos t + q\sin t)$, where q is dependent on the nonlinear coefficients of the normal form. If $q = 0$, the isochrons are radial; otherwise they have a twist. The desired integral is $-q$, so that if $q > 1$, then even with this special coupling, synchrony will be unstable. It is for this reason that we cannot say anything general about when synchrony is stable near a Hopf bifurcation, except that for systems with nearly radial isochrons, where we can say that synchrony is an attractor.

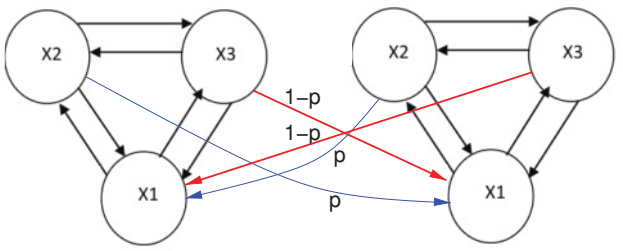

FIG. 8. (Color online) Example of a symmetric coupling motif with composite coupling.

C. Interaction functions for circulant systems

The general interaction function for two coupled motifs has the form

$$H(\phi) = -\frac{1}{P}\int_0^P \left[\sum_{i,j=1}^{m} z_i(t) C_{ij} x_j(t+\phi)\right] dt,$$

where the functions $x_i(t), z_i(t)$ are very general and bear little relationship to each other. However, in a circulant system, the translational symmetry leads to the bifurcation to patterns of activity that are identical to traveling waves, cf. Fig. 6(c). This means that the only difference between, say, $x_i(t)$ and $x_j(t)$, is a temporal phase shift. That is, there exists an integer k such that $x_j(t) = x_i(t + kP/m)$, where m is the number of neurons in the motif and P is the period of the oscillation. Similarly, the sensitivities $z_i(t)$ are related in the same way. Hence, to compute the interaction, we need only compute one integral and the rest will just be phase shifts. Specifically, let k_i be such that $x_i(t) = x_1(t + k_i P/m)$ and $z_i(t) = z_1(t + k_i P/m)$. Consider a term in the interaction function of the form

$$-\frac{1}{P}\int_0^P C_{ij} z_i(t) x_j(t+\phi) dt.$$

We can rewrite this as

$$-\frac{1}{P}\int_0^P C_{ij} z_1(t + k_i P/m) x_1(t + k_j P/m + \phi) dt,$$

which is then

$$-C_{ij}\frac{1}{P}\int_0^P z_1(t) x_1(t + (k_j - k_i)P/m + \phi) dt.$$

Let

$$h(\phi) := -\frac{1}{P}\int_0^P z_1(t) x_1(t+\phi) dt.$$

Then the general interaction function has the form

$$H(\phi) = \sum_{i,j=1}^{m} C_{ij} h\left(\phi + P\frac{k_j - k_i}{m}\right).$$

Thus, for circulant motifs, the composite interaction function is a weighted sum of the phase shift of the single $1 \to 1$ connection. In particular, we need only study coupled networks

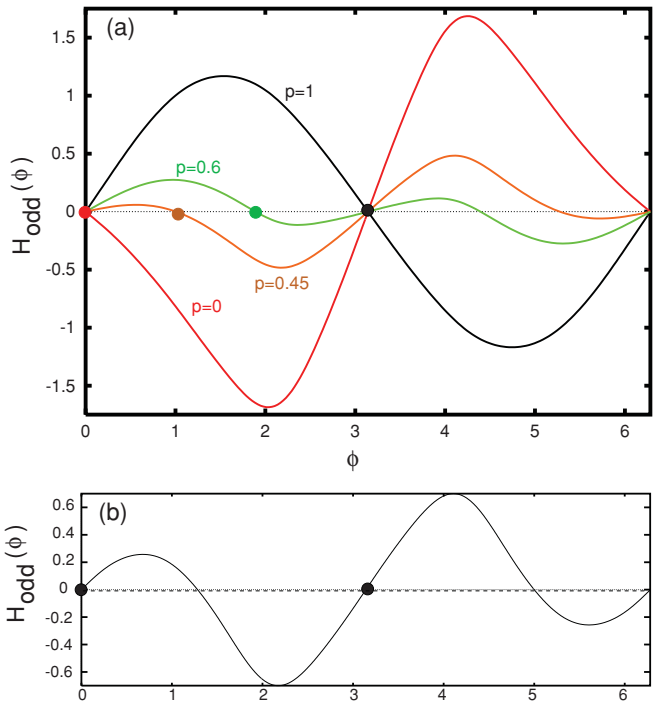

FIG. 9. (Color online) (a) $-2h_p^o(\phi)$, where h_p^o is the odd part of the weak-coupling function for the composite coupling illustrated in Fig. 8. Filled circles show stable fixed points for four different values of p. (b) Odd part of the H function when the connection is #1 to #1.

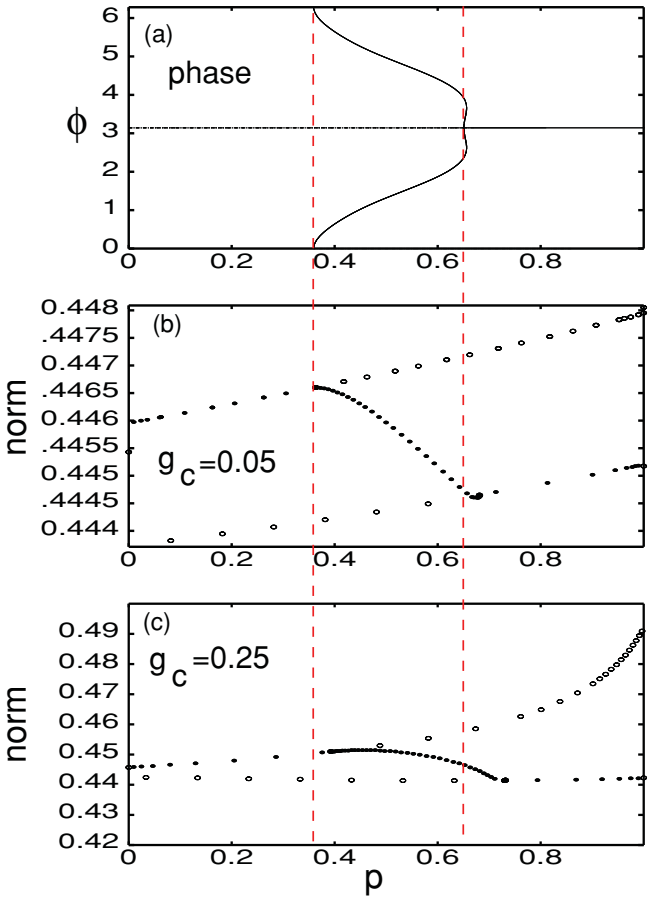

FIG. 10. (Color online) Behavior of the phase model and the full model as p varies. (a) Equilibria for the phase equation. (b), (c) Norm of periodic solutions to the full model for two different coupling magnitudes.

where a single cell in the motif (call it cell 1) receives all the inputs from the other motif. For example, in the simplest three-cell motif, we need to look only at the cases where C_{11}, C_{12}, C_{13} are nonzero and thus

$$H(\phi) = C_{11}h(\phi) + C_{12}h(\phi + P/3) + C_{13}h(\phi - P/3), \quad (13)$$

where we use that fact that $2P/3 = -P/3$ modulo P.

IV. SYNCHRONY AND LOCKING IN CIRCULANT SYSTEMS

We start this section with an exploration of the dynamics of a pair of coupled three-cell motifs. From the discussion in the previous section and Eq. (13), we need only look at networks in which cell 1 receives all the inputs. Figure 8 shows an example system in which cell 1 receives input only from cells 2 and 3 in the other motif. When $p = 1$, coupling is just from 2 to 1, and when $p = 0$, it is from 3 to 1. We set

$$H_p(\phi) = ph(\phi + P/3) + (1 - p)h(\phi - P/3).$$

The phase difference between the two motifs satisfies

$$\frac{d\phi}{dt} = -2h_p^{\text{odd}}(\phi) := H_p(-\phi) - H_p(\phi).$$

Figure 9(a) shows h_p^{odd} for several different values of p. When $p = 1$ and connections are only from 2 to 1, the antiphase solution is the only stable equilibrium and we expect that for weak coupling the two motifs will oscillate out of phase. In contrast, when $p = 0$ and coupling is only from 3 to 1, then perfect synchrony is an asymptotically stable solution; the two motifs will synchronize. For a mixture of the two types of coupling, the stable phase difference between the two networks can take many values between synchrony and antiphase. Thus, the timing difference (phase difference) between the two symmetrically coupled networks can be arbitrarily prescribed by adjusting the ratio of the coupling strengths between different members of the motif. Figure 10(a) formalizes this idea by showing the stable equilibria for the weakly coupled pair of networks as a function of the parameter p. When $p = 0$, synchrony is stable. As p increases, there is a supercritical pitchfork bifurcation for $p \approx 0.35$. The new branch of stable solutions represents a state in which the stable phase difference between the two oscillatory networks is some intermediate value that increases from $\phi = 0$ in a monotonic fashion as p increases past 0.35. Starting at the other extreme, when $p = 1$, the antiphase solution is stable. As p decreases, the antiphase solution loses stability for $p \approx 0.65$. There is a subcritical pitchfork bifurcation which "turns around" to become supercritical, where it joins with the solution branch

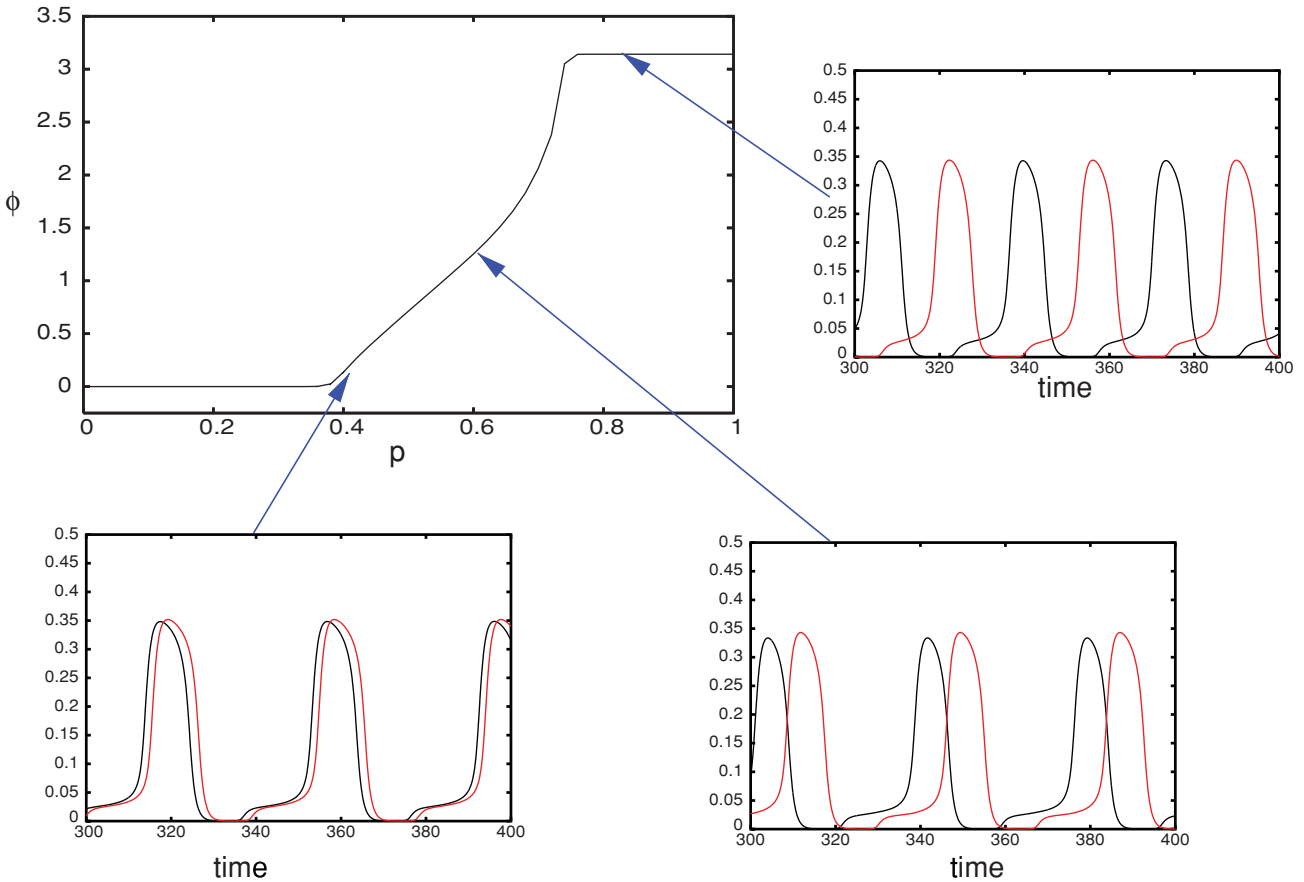

FIG. 11. (Color online) Phase shift between the two three-cell systems as a function of p for $g_c = 0.25$. Phase shift is defined as follows. Let t_1 be the time at which unit 1 in system X crosses 0.2; let t_2 be the time at which unit 1 in system Y crosses 0.2; let t_3 be the next time that unit 1 in system X crosses 0.2. The phase shift is $2\pi(t_2 - t_1)/(t_3 - t_1)$.

emerging from the synchronous solution. Thus, except for a small interval of phases near the antiphase solution, it is possible to achieve an arbitrary stable phase difference between the two networks by doing nothing more than varying the coupling ratio between the two connections. More generally, suppose we have two types of coupling, say, $H_0(\phi)$ and $H_1(\phi)$, and consider $H_p(\phi) = (1-p)H_0(\phi) + pH_1(\phi)$. Suppose that $H_0'(0) = a_0 > 0$ and $H_0'(P/2) = -b_0 < 0$. This means that with $p = 0$, synchrony is stable and antiphase is unstable. Suppose, in contrast, that $H_1'(0) = -a_1 < 0$ and $H_1'(P/2) = b_1 > 0$. That is, when $p = 1$, synchrony is unstable and antiphase is stable. Then we can compute the value of p for the pitchfork to occur on these branches. Synchrony ($\phi = 0$) is unstable for $p > a_1/(a_1 + a_0) := p_s$ and antiphase is unstable for $p < b_1/(b_0 + b_1) := p_a$. Generically, the pitchfork will not be degenerate. [For example, let $p = p_s$ be the value of p where synchrony loses stability. Let $h_{\text{odd}}(\phi)$ be the odd part of H at this value of $p = p_s$. Then $h'_{\text{odd}}(0) = 0$ is the condition for the loss of stability. The condition for a nondegenerate pitchfork is $h'''_{\text{odd}}(0) \neq 0$. The sign of this quantity determines whether or not the pitchfork is subcritical or supercritical. A similar condition holds at $p = p_a$.]

In our particular case, the new solutions which bifurcated from synchrony and antiphase were stable and represented an intermediate phase difference. However, it is not necessary for this to happen. Instead, for example, suppose that $p_a < p_s$. Then for $p_a < p < p_s$, both antiphase and synchrony are stable. The coupled network is bistable. It turns out that in our canonical three-cell circuit, the single reciprocal connection from 1 to 1 provides a bistable system with both synchrony and antiphase stable, as seen in Fig. 9(b).

In sum, a weak-coupling analysis shows that *even with symmetric coupling of identical oscillators*, it is possible to modulate the phase difference between a coupled pair of networks by just varying the coupling ratio, that is, who is coupled to whom.

A. Beyond weak coupling

While the results for weak coupling show the rich possibilities of interacting circulant motifs, it is not clear how robust the timing and phase differences will be as the strength of coupling increases and the full oscillatory networks become more distorted due to the coupling. In Figs. 10(b) and 10(c), we show bifurcation diagrams for coupling between units with strength $g_c = 0.05, 0.25$ as p varies. In both cases, synchrony is stable for p small and antiphase is stable for p close to 1. As with the phase model, both the synchronous and antiphase solutions lose stability via a pitchfork and the critical values of p are close to those predicted through weak-coupling theory. Figure 11 shows the timing difference between the corresponding unit 1's in the two networks with moderate-coupling strength. As predicted from weak-coupling theory, synchrony and antiphase disappear for p between 0.4 and 0.7 and the timing difference (or phase; details on how this is computed are in the figure legend) can take on any value. In particular, the timing is uniquely determined by p. Typical time series at three values of p are shown. For $p = 0.6$, the oscillation is somewhat distorted as the firing rates are not simply phase shifts of each other, rather, their amplitudes are also different.

Figure 12 summarizes the global dynamics as the coupling strength g_c increases. In Fig. 12(a), stability of synchrony is lost through a pitchfork bifurcation as p changes for all coupling strengths, $g_c < 0.52$. For $g_c > 0.52$, synchrony is stable for all p. Furthermore, synchrony restabilizes as p increases for coupling larger than $g_c \approx 0.3$. Figure 12(b) shows an analogous diagram for the fate of the antiphase branch. Pitchfork bifurcations occur (with respect to the parameter p) for coupling strengths up to between 0.5 and 0.65. Beyond that, the antiphase branch is lost to a saddle-node bifurcation.

One of the main points of this paper is that an architecture in which cells within a motif come on at different times in the cycle can allow coupled networks to stably maintain specific phase relationships. However, it might be the case that these phase relationships (except synchrony and antiphase) are very sensitive to the frequency of the oscillations. Thus, we consider the network shown in the last two figures, but now let the current input I change between $I = 1$ and $I = 2$. At $I = 1$, the uncoupled system is near the Hopf bifurcation and the amplitude of the oscillation is very small, while when $I = 2$, it is close to the SNIC and the amplitude is quite large. The period ranges from ~10 to ~50. In spite of this large range in amplitude and period, for a fixed interaction between the two subnetworks (that is, for fixed p), the phase is remarkably

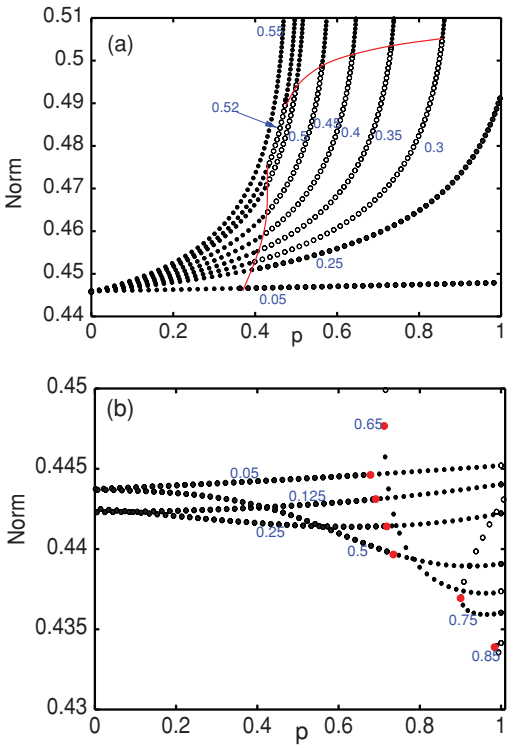

FIG. 12. (Color online) "Two-parameter" diagram for the full model. (a) Fate of the synchronous solution as p changes for different coupling strengths. A curve is drawn through the values of the pitchfork bifurcation. (b) Fate of the antiphase branch as p changes for different coupling strengths. Circles show the bifurcation points at pitchfork or saddle-node bifurcations.

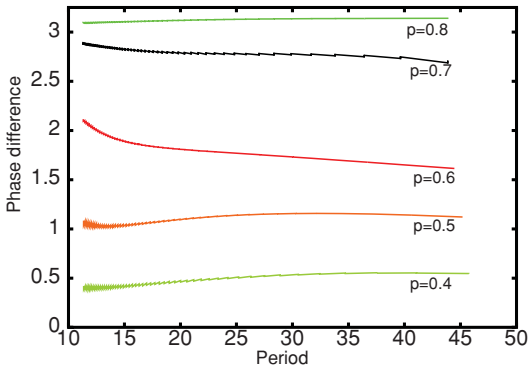

FIG. 13. (Color online) Robustness of the phase-difference as a function of the period of the oscillation. Phase shift between the two firing rate models when $g_c = 0.05$ and the input current I to each unit varies between $I = 1$ and $I = 2$.

constant. Figure 13 shows the phase difference (as measured in Fig. 11) as the period varies (achieved by changing the input I). For each choice of p, the phase is almost constant over the entire range of periods.

B. Noncirculant systems

Symmetric connectivity between circulant systems has been shown to yield the possibility for arbitrary time differences between pairs of the motifs. We explored in great detail the dynamics of a specific three-neuron circulant system. However, the basic principle that underlies this, shared activity that occurs at different times during the cycle, should hold in any inhibitory network. For example, consider the random 20-cell network shown in Fig. 5 at the parameter value shown by the arrow. Figure 14 shows a summary of the dynamics predicted from weak coupling and the actual dynamics of a pair of two 20-neuron systems. Figure 14(a) shows the spatiotemporal pattern of dynamics over a period of time. The uncoupled period of the network is 8.4. While lacking the symmetry of a circulant system, it is clear that different neurons come on at different times during the cycle. Figure 14(b) shows the adjoint $X^*(t)$ for the network over one cycle. The arrow marks the sensitivity for oscillator No. 4 and its time series is shown in Fig. 14(c) along with the activity profile of oscillator No. 7 [arrow in Fig. 14(a)]. We compute the odd part of the interaction function when the two systems are coupled via a single symmetric interaction where unit No. 4 receives an input from one of several different units. Weak coupling theory predicts that if the interaction is from No. 1, then the two systems oscillate in antiphase, while if it is from No. 15, they will synchronize. Interactions mediated by No. 7 or No. 4 are predicted to lead to phase locking at an intermediate phase difference. (Recall that roots of the odd part of the interaction are possible phase-locked times and that the root is

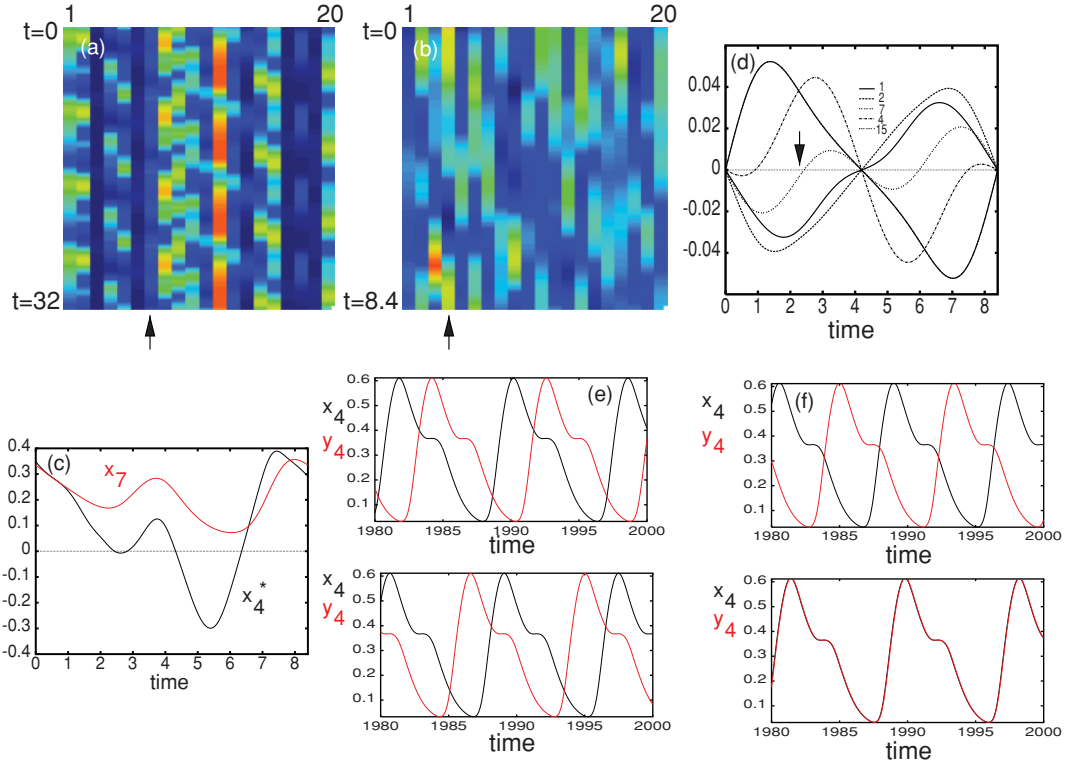

FIG. 14. (Color online) Dynamics of the network from Fig. 5. (a) Several cycles (time goes down) showing activity of neurons in the network. (b) Adjoint for one cycle of the oscillation in (a). (c) Plot of the adjoint $x_4^*(t)$ [shown by the arrow in (b)] and the activity $x_7(t)$ [arrow in (a)]. (d) Odd part of the interaction function from weak-coupling theory when one each of five different units is connected to unit No. 4. (e) Simulation of a pair of coupled 20-cell WLC systems ($g_c = 0.05$) where No. 7 connects to No. 4. Two different steady states are shown showing the symmetry of the system. (f) Coupling from No. 2 to No. 4 leads to antiphase oscillations (top) and No. 15 to No. 4 leads to synchrony (bottom).

stable if the slope of the odd part of the interaction function is positive.) Figure 14(e) shows the dynamics of the full model when coupling between the two systems is 0.05. Two different initial conditions lead to two different patterns corresponding to each of the two systems taking a small lead. [The curve in Fig. 14(d) marked by the arrow has two roots with a positive slope.] Figure 14(f) shows simulations for coupling between No. 1 and No. 4 (top, antiphase) and No. 15 and No. 4 (bottom, synchronous). Thus, we see that it is not necessary to have a circulant system in order for the ideas in this section to be relevant. What matters is not the symmetry but the mere fact that different components of the network turn on at different times during the cycle.

V. CONCLUSION

Many neural systems consist of repetitions of similar motifs that are then coupled together in order to form patterns of activity that may be useful for some types of computations or for creating desirable motor outputs. In this paper, we consider a specific type of motif that is dominated by nonsymmetric recurrent inhibition. We showed that such networks were capable of producing wavelike repetitive activity even in absence of any spatial organization. We then showed that it is possible to design reciprocal symmetric coupling between pairs of these motifs such that they are able to produce arbitrary timing differences. Such timing differences are quite important in CPGs which are responsible for producing rhythmic patterned output to muscles used in locomotion and many other behaviors. For example, the crayfish swimmeret system requires a phase difference of a quarter of a cycle between each of the four segments that comprise the pattern generator [8]. This phase difference must be maintained over a wide range of swimming speeds corresponding to a similar range in oscillatory frequencies. Similarly, the lamprey spinal cord consists of $\sim$100 segments, each of which consists of many reciprocally connected inhibitory neurons [28]. These segments must be coupled in such a way that they maintain a precise phase lag independent of the swimming speed of the animal [7]. Simple motifs of the type described in this paper have exactly this property. As many CPGs are composed of networks of mutually inhibitory neurons, the architecture in this paper could provide a simple robust mechanism for keeping a constant intersegmental phase lag over the entire range of physiological frequencies.

There have been other attempts at analyzing networks of inhibitorily coupled neurons. A recent paper, Ref. [29], considers the stability and dynamics of a large network consisting of coupled WTA systems. In this work the authors coupled these motifs and use contraction theory to analyze how the stability of the resulting patterns depends on the connectivity. Reference [30] studied clustering and other dynamics in coupled five-cell motifs where each isolated motif generates rhythmic and cyclic dynamics. What Ashwin terms as WLC refers to slow switching between cluster states. This phenomena occurs if the system has a very specific interaction function which is perturbed by a small amount of noise. Reference [15] used a singular perturbation theory to analyze the global dynamics of networks of inhibitorily coupled neurons. Terman *et al*. studied inhibitory networks which exhibit dynamic clustering. The time evolution of these networks is divided into episodes. During every episode neurons in these networks fire due to postinhibitory rebound. These networks can produce a variety of periodic sequences which are dependent on the initial conditions of the system. Reference [31] analyzed networks similar to our three-cell circulant system using harmonic balance and perturbation theory. Chen's neurons are coupled differently than ours in that they are coupled unidirectionally. His model also includes excitation. This system displays similar dynamics to ours except that he approximates all of his membrane potentials as pure sinusoids. Our approach has been to use a weak-coupling analysis of networks of motifs, each of which is an oscillator that depends on strong recurrent inhibition. Our canonical motif is the three-neuron circulantly coupled system. A similar system was studied by Rabinovich [32]. His work, however, focused on the creation of a heteroclinic cycle from a bifurcation due to asymmetry in the synaptic conductances. Our analysis is a general study of limit cycle behavior in systems coupled with circulant matrices. Our perturbed limit cycles are fundamentally different than a heteroclinic cycle.

The methods and ideas in this paper are not restricted to neural applications. The repressilator [33,34] is a synthetic genetic circuit which produces sustained oscillations. The mechanism is an asymmetric negative feedback loop between three genes, essentially identical in structure and behavior to Eq. (3). Thus, the ideas in this paper could also be used to set up arbitrary spatiotemporal patterns in oscillating cellular networks.

[1] R. J. Prill, P. A. Iglesias, and A. Levchenko, PLoS Biol. **3**, e343 (2005).

[2] O. Sporns and R. Kotter, PLoS Biol. **2**, e369 (2004).

[3] A. A. Prinz, D. Bucher, and E. Marder, Nat. Neurosci. **7**, 1345 (2004).

[4] A. L. Weaver and S. L. Hooper, J. Neurophysiol. **90**, 2378 (2003).

[5] A. G. Bulloch and N. I. Syed, Trends Neurosci. **15**, 422 (1992).

[6] A. Shilnikov, R. Gordon, and I. Belykh, Chaos **18**, 037120 (2008).

[7] P. L. Varkonyi, T. Kiemel, K. Hoffman, A. H. Cohen, and P. Holmes, J. Comput. Neurosci. **25**, 245 (2008).

[8] S. R. Jones, B. Mulloney, T. J. Kaper, and N. Kopell, J. Neurosci. **23**, 3457 (2003).

[9] P. D. Brodfuehrer, E. A. Debski, B. A. O'Gara, and W. O. Friesen, J. Neurobiol. **27**, 403 (1995).

[10] J. Collins and I. Stewart, J. Nonlinear Sci. **3**, 349 (1993).

[11] Carla M. A. Pinto and Martin Golubitsky, J. Math. Biol. **53**, 474 (2006).

[12] J. E. Rubin, N. A. Shevtsova, G. B. Ermentrout, J. C. Smith, and I. A. Rybak, J. Neurophysiol. **101**, 2146 (2009).

[13] Mikhail I. Rabinovich, Pablo Varona, Allen I. Selverston, and Henry D. I. Abarbanel, Rev. Mod. Phys. **78**, 1213 (2006).

[14] A. Szucs, R. Huerta, M. I. Rabinovich, and A. I. Selverston, Neuron **61**, 439 (2009).
[15] D. Terman, S. Ahn, X. Wang, and W. Just, Physica D **237**, 324 (2010).
[16] M. S. Goldman, Neuron **61**, 621 (2009).
[17] B. K. Murphy and K. D. Miller, Neuron **61**, 635 (2009).
[18] M. Bazhenov, M. Stopfer, M. Rabinovich, H. D. Abarbanel, T. J. Sejnowski, and G. Laurent, Neuron **30**, 569 (2001).
[19] M. d. C. A. Leite and M. Golubitsky, Nonlinearity **19**, 2313 (2006).
[20] M. Golubitsky, I. Stewart, and A. Török, SIAM J. Appl. Dyn. Syst. **4**, 78 (2005).
[21] K. Rajan and L. F. Abbott, Phys. Rev. Lett. **97**, 188104 (2006).
[22] J. J. Hopfield, Proc. Natl. Acad. Sci. USA **79**, 2554 (1982).
[23] R. Ben-Yishai, D. Hansel, and H. Sompolinsky, J. Comput. Neurosci. **4**, 57 (1997).
[24] E. Izhikevich, *Dynamical Systems in Neuroscience: The Geometry of Excitabilty and Bursting* (MIT Press, Cambridge, MA, 2007).
[25] G. B. Ermentrout and N. Kopell, SIAM J. Math. Anal. **15**, 215 (1984).
[26] Y. Kuramoto, *Chemical Oscillations, Waves, and Turbulence* (Springer, New York, 1984).
[27] G. B. Ermentrout and N. Kopell, SIAM J Appl. Math. **46**, 233 (1986).
[28] J. H. Kotaleski, S. Grillner, and A. Lansner, Biol. Cybern. **81**, 317 (1999).
[29] U. Rutishauser, R. Douglas, and J.-J. Slotine, Neural Comput. **23**, 735 (2011).
[30] G. Orosz, P. Ashwin, and S. Townley, IEEE Trans. Neural Netw. **20**, 1135 (2009).
[31] Z. Chen, M. Zheng, W. O. Friesen, and T. Iwasaki, J. Comput. Neurosci. **25**, 583 (2008).
[32] T. Nowotny and M. I. Rabinovich, Phys. Rev. Lett. **98**, 128106 (2007).
[33] M. B. Elowitz and S. Leibler, Nature (London) **403**, 335 (2000).
[34] S. Müller, J. Hofbauer, L. Endler, C. Flamm, S. Widder, and P. Schuster, J. Math. Biol. **53**, 905 (2006).